

## Rothamsted Repository Download

### A - Papers appearing in refereed journals

Wu, L., Curceac, S., Atkinson, Peter, Milne, A. E. and Harris, P. 2021. A case study on the effects of data temporal resolution on the simulation of water flux extremes using a process-based model at the grassland field scale. *Agricultural Water Management*. 255.  
<https://doi.org/10.1016/j.agwat.2021.107049>

The publisher's version can be accessed at:

- <https://doi.org/10.1016/j.agwat.2021.107049>

The output can be accessed at: <https://repository.rothamsted.ac.uk/item/98571/a-case-study-on-the-effects-of-data-temporal-resolution-on-the-simulation-of-water-flux-extremes-using-a-process-based-model-at-the-grassland-field-scale>.

© 2 July 2021, Please contact [library@rothamsted.ac.uk](mailto:library@rothamsted.ac.uk) for copyright queries.

1 **A case study on the effects of data temporal resolution on the simulation of water**  
2 **flux extremes using a process-based model at the grassland field scale**

3 Lianhai Wu <sup>a,\*</sup>, Stelian Curceac <sup>a</sup>, Peter M. Atkinson <sup>b,c,d</sup>, Alice Milne <sup>e</sup>, Paul Harris <sup>a</sup>  
4

5 <sup>a</sup> Rothamsted Research, Department of Sustainable Agriculture Sciences, North Wyke EX20 2SB, Devon, UK.

6 <sup>b</sup> Lancaster Environment Centre, Lancaster University, Lancaster LA1 4YQ, UK.

7 <sup>c</sup> Geography and Environment, University of Southampton, Highfield, Southampton SO17 1BJ, UK.

8 <sup>d</sup> State Key Laboratory of Resources and Environmental Information System, Institute of Geographical Sciences and Natural  
9 Resources Research, Chinese Academy of Sciences, Beijing 100101, China.

10 <sup>e</sup> Rothamsted Research, Department of Sustainable Agriculture Sciences, Harpenden AL5 2JQ, UK  
11

12 \* Corresponding author: Lianhai Wu

13 Email: [lianhai.wu@rothamsted.ac.uk](mailto:lianhai.wu@rothamsted.ac.uk)

14

## 15 **Abstract**

16 Projected changes to rainfall patterns may exacerbate existing risks posed by flooding.  
17 Furthermore, increased surface runoff from agricultural land increases pollution through  
18 nutrient losses. Agricultural systems are complex because they are managed in individual  
19 fields, and it is impractical to provide resources to monitor their water fluxes. In this respect,  
20 modelling provides an inexpensive tool for simulating fluxes. At the field-scale, a daily time-  
21 step is used routinely, however, it was hypothesized that a finer time-step will provide more  
22 accurate identification of peak fluxes. To investigate this, the process-based SPACSYS  
23 model that simulates water fluxes, soil carbon and nitrogen cycling as well as plant growth  
24 with a daily time-step was adapted to provide sub-daily simulations. As a case study, the  
25 water flux simulations were checked against a 15-minute measured water flux dataset from  
26 April 2013 to February 2016 from a pasture within a monitored grassland research farm,  
27 where the data were up-scaled to hourly, 6-hourly and daily. Analyses were conducted with  
28 respect to model performance for: (a) each of the four data resolutions, separately (15-minute  
29 measured versus 15-minute simulated; hourly measured versus hourly simulated; etc.); and  
30 (b) at the daily resolution only, where 15-minute, hourly and 6-hourly simulations were each  
31 aggregated to the daily scale. Comparison between measured and simulated fluxes at the four  
32 resolutions revealed that hourly simulations provided the smallest misclassification rate for  
33 identifying water flux peaks. Conversely, aggregating to the daily scale using either 15-  
34 minute or hourly simulations increased accuracy, both in prediction of general trends and  
35 identification of peak fluxes. For the latter investigation, the improved identification of  
36 extremes resulted in 9 out of 11 peak flow events being correctly identified with only 2 false  
37 positives, compared with 5 peaks being identified with 4 false positives of the usual daily  
38 simulations. Increased peak flow detection accuracy has the potential to provide clear field  
39 management benefits in reducing nutrient losses to water.

40 **Key words:** SPACSYS; extreme flows; North Wyke Farm Platform; scale effects; grassland;

41

## 42 **1 Introduction**

43 Flooding in the UK puts more than 5 million people in 2.4 million properties at risk each year  
44 (Environment Agency, 2009). Projected changes to rainfall patterns (Watts and Anderson,  
45 2016) may exacerbate the existing risks posed by flooding. Flash flooding or surface water  
46 flooding, defined as those flood events where the rise in water is either during or within a few  
47 hours of the rainfall that produces the rise, is one of the most common types of flooding in  
48 the UK. The utilised agricultural area, of which almost 60% is permanent grassland, covers  
49 71% of the total land of the UK (Department for Environment, Food and Rural Affairs,  
50 2019). Water fluxes or surface runoff generated from agricultural land can contribute  
51 significantly to local floods and nutrient losses that cause water pollution. Flooding of  
52 farmland is likely to become more frequent in some areas under projected climate change  
53 (Brown et al., 2016), although intriguingly, studies have found increases in precipitation  
54 extremes do not necessarily mean increases in flood magnitude, due to decreased soil  
55 moisture at storm onset and reduced storm durations (Sharma et al., 2018; Wasko et al.,  
56 2019). Further, soil erosion is accelerating due to more intense rainfall, leading to the loss of  
57 valuable topsoil and the pollution of watercourses (Morison and Matthews, 2016).

58

59 Accurate forecasting of water runoff (or water fluxes) from agricultural land is, therefore, not  
60 only a vital component of flood early-warning systems, but also for associated management  
61 strategies for nutrient loss and water pollution. Water fluxes from the soil surface are  
62 controlled by soil properties. Long-term hydrological studies have shown that sandy Alfisols  
63 can generate higher runoff compared to clayey Vertisols (Pathak et al., 2013), and a greater

64 risk of flooding on clay soils has been reported (Charlton et al., 2010). The wetness of the soil  
65 before a precipitation event (Merz and Plate, 1997) and soil compaction also affect water  
66 fluxes. Farm machinery and livestock (Adimassu et al., 2019; Alaoui et al., 2018; Newell  
67 Price et al., 2012) can cause serious compaction and so exacerbate flood risk. Natural events,  
68 particularly long and intense precipitation events (Archer and Fowler, 2018), and land cover  
69 variation (Dadson et al., 2017; Keesstra et al., 2018) also affect flux.

70

71 Agricultural systems are complex because they are generally managed at the field scale and  
72 each field has its own unique set of soil conditions and topology. Monitoring water surface  
73 fluxes in fields is costly both in time and financially. In this respect, modelling provides an  
74 effective tool for simulating or forecasting water fluxes. The SPACSYS model (Wu et al.,  
75 2007) is one such process-based model. It is a field scale and weather-driven dynamic  
76 simulation model. Since it was first published in 2007, it has been developed to provide  
77 added functionality (Bingham and Wu, 2011; Liu et al., 2013; Wu et al., 2019; Wu et al.,  
78 2015). The model can simulate the interactions of soil carbon (C), nitrogen (N) and  
79 phosphorus (P), plant growth and development, water re-distribution and heat transformation  
80 in agricultural fields. The model has been used to investigate several issues including  
81 resource use efficiency by crops (Wu et al., 2009), greenhouse gas (GHG) emissions (Abalos  
82 et al., 2016; Perego et al., 2016), the responses of cropping/grassland systems to  
83 environmental change (Wu et al., 2016) and the forecasting of crop yield and stocks of C and  
84 nutrients (Zhang et al., 2016) under various climatic and soil conditions.

85

86 The SPACSYS model has been developed to investigate not only temporal dynamics, but  
87 also within-field spatial variation in processes such as water runoff, using a linked, grid-based

88 approach (grid-to-grid) (Liu et al., 2018). As in all previous implementations of SPACSYS,  
89 and common to many agriculture-focused models (Ahuja et al., 2002), a daily time-step was  
90 used. However, model predictions of water flux did not increase in accuracy when  
91 considering grid connectivity. We hypothesise, that a finer time-step might provide this  
92 improvement instead; not only in the grid-to-grid model, but also in the (non-grid-to-grid)  
93 standard model, as investigated here. Although not demonstrated within this study, increasing  
94 the accuracy of water flux simulations should implicitly increase the accuracy of associated  
95 SPACSYS simulations, such as those for nutrient loss that use predicted water flux in their  
96 calculation.

97

98 For our case study, we used measured 15-minute water flux data from one field (or sub-  
99 catchment) of the North Wyke Farm Platform (NWFP). The NWFP is a systems scale  
100 research facility in the south-west of England for investigation of the sustainability of  
101 lowland ruminant production systems (Orr et al., 2016). South-west England has a relatively  
102 wet climate where the greatest rainfall is in winter and the driest times are between April to  
103 July. August tends to show an increase in rainfall over July and starts the inexorable rise in  
104 rainfall into autumn and early winter. More recently, the number of flood events has  
105 increased (Stevens et al., 2016), mostly in the autumn and winter months; all as a likely  
106 consequence of increased surface water runoff (Palmer and Smith, 2013).

107

108 For this study, the NWFP's 15-minute water flux data were up-scaled to hourly, 6-hourly and  
109 daily data and the SPACSYS model was adapted to provide corresponding downscaled  
110 simulations at 15-minute, hourly and 6-hourly resolutions (in addition to its usual daily  
111 output). This provided four measured water flux datasets and four simulated water flux

112 datasets over a study period of 34 months (April 2013 to February 2016). Simulations were  
113 generated using the same field management practices and parameter configurations. These  
114 rich water flux datasets enabled investigation of the effects of temporal scale on model  
115 performance not only in terms of extreme water runoff, which is the study focus and provides  
116 it's novelty, but also in terms of general trends.

117

## 118 **2 Materials and Methods**

### 119 *2.1 Model description*

120 The SPACSYS model includes a plant growth and development component, an N cycling  
121 component, a C cycling component, a P cycling component, plus a soil water component that  
122 includes representation of water flow to field drains as well as downwards through the soil  
123 layers, together with a heat transfer component. The equations to quantify such different  
124 processes have been described elsewhere (Liu et al., 2013; Wu et al., 2019; Wu et al., 2007;  
125 Wu et al., 2015). Here, only the processes influencing directly the soil water component are  
126 presented.

127

128 For SPACSYS, the Richard's equation for water potential and Fourier's equation for  
129 temperature are used to simulate water and heat fluxes, which are inherited from the SOIL  
130 model (Jansson, 1998). If the water content in a layer rises above a specified value a  
131 proportion is held in macropores such that rapid downward water movement takes place due  
132 to gravitational forces alone. Water flow from the soil profile to a drainage pipe occurs when  
133 the ground water table is above the bottom level of the pipe and the soil below the ground  
134 water table is saturated. The Hooghoudt drainage flow equation with modification is adopted  
135 for the subsurface drainage flow.

136

137 The main processes concerning plant growth in SPACSYS are plant development,  
138 assimilation, respiration, root growth and development, water uptake, nutrient uptake,  
139 biological N fixation for legume plants and partitioning of photosynthate and nutrients from  
140 uptake estimated with various mechanisms implemented in the model. N cycling coupled  
141 with C cycling covers the transformation processes for organic matter and inorganic N. The  
142 main processes and transformations causing size changes to mineral N pools are  
143 mineralization, nitrification, denitrification including N gaseous emission and plant N uptake.  
144 P cycling is linked to other components such as the plant component, heat transformation and  
145 the water cycle. Organic P is subdivided into certain sub-pools with different forms which are  
146 connected with transformation rates.

147

## 148 2.2 *The North Wyke Farm Platform*

149 The study site is located in south-west England, at the NWFP, Rothamsted Research,  
150 Okehampton, Devon (50°46'10''N, 30°54'05''W). For the period 1985-2015, the mean  
151 annual temperature in North Wyke ranges between 6.8 and 13.4 °C, the mean annual rainfall  
152 is 1033 mm and the climate is classed as cool temperate. The platform is a 63 ha systems-  
153 based experimental facility divided into 15 hydrologically isolated sub-catchments across  
154 three 21 ha farmlets with five sub-catchments in each. At the time of this study, all three  
155 farmlets were used solely for grazing livestock research (sheep and cattle) where each farmlet  
156 was operating under different sward management strategies: no re-seeding (permanent  
157 pasture); re-seeded monoculture; and re-seeded legume mix. The platform monitors routinely  
158 water runoff and water chemistry in each of the 15 sub-catchments, together with other  
159 primary data collections (e.g. greenhouse gas emissions, livestock performance) so that each

160 farming system can be described, contrasted and compared according to its level of  
161 sustainability (Orr et al., 2016). Datasets are freely available from  
162 <https://www.rothamsted.ac.uk/north-wyke-farm-platform>, including those used in this study.

163

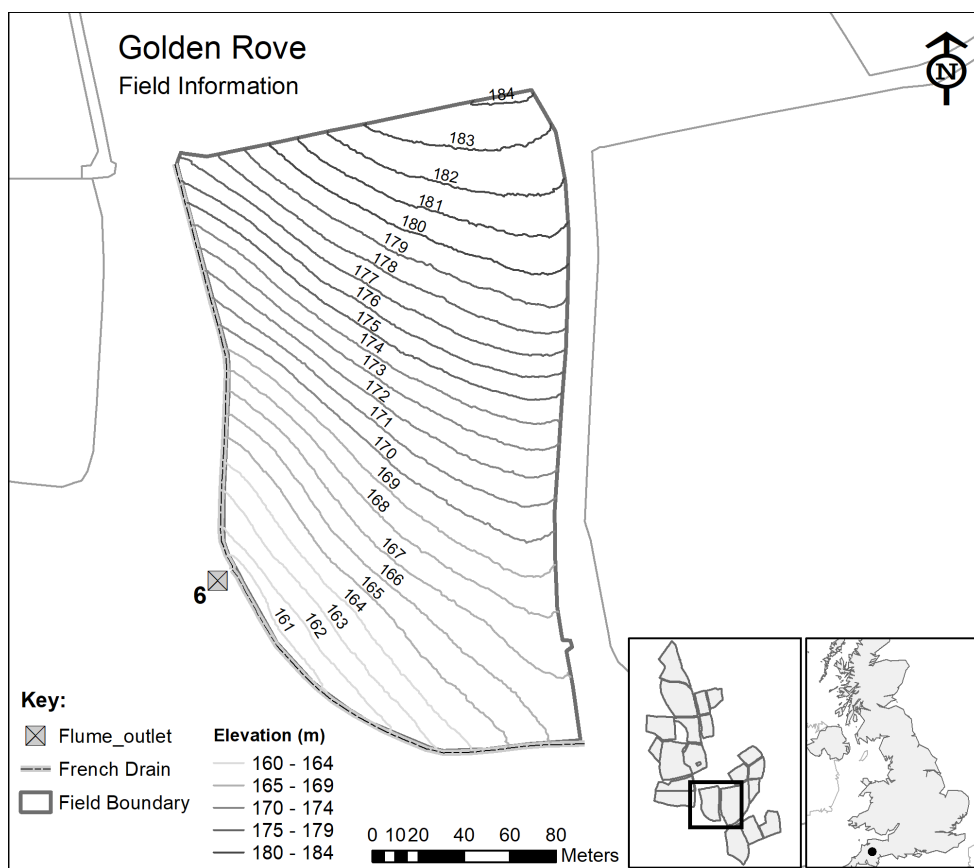
### 164 2.3 *Model configuration*

165 For this study, we focused on water fluxes for one sub-catchment in the permanent pasture  
166 farmlet called 'Golden Rove'; a single field that has been under permanent pasture since the  
167 outset of the platform in 2010 (Fig. Figure 1). The soil class for this field is primarily  
168 Halstow, which comprises a slightly stony clay loam topsoil (approximately 36% clay) that  
169 overlies a mottled stony clay (approximately 60% clay), derived from underlying  
170 Carboniferous Culm rocks (Harrod and Hogan, 2008). The study field also has a smaller, but  
171 not insignificant area of Denbigh-Cherubier soil class. In the simulations, the soil type was  
172 ignored.

173

174 To mimic the grazing system, daily grass intake and excretion of sheep and cattle in the field  
175 was estimated before running the simulations (Carswell et al., 2019; Wu et al., 2016). Soil  
176 physical and chemical properties of the field were adopted from a previous study of the same  
177 field (Wu et al., 2016). The temporal frequency for the measured water fluxes ( $l\ s^{-1}$ ) from a  
178 NWFP water flume has been 15-minutes since the outset of the platform's setup in October  
179 2012. However, meteorological measurements at the same 15-minute resolution were only  
180 initiated from 30 April 2013. Thus, to ensure consistency in the frequency of the driving  
181 variables and the water flux as an output variable, simulations also started from 30 April  
182 2013. An end-date of 15 February 2016 was chosen to give an interrupted data collection  
183 time period of 34 months. A longer time period would entail having significant periods of

184 missing data due to instrument failure (i.e. there were no measurements on water flux  
185 between 15 February and 24 October 2016). A previous scale-focused study, analysing the  
186 measured 15-minute water fluxes together with aggregations at 30-minute, hourly, 3-hourly,  
187 6-hourly, 12-hourly and daily resolutions, indicated that 15-minute, hourly, 6-hourly and  
188 daily resolutions is sufficient to communicate all key outcomes adequately (Curceac et al.,  
189 2020). Thus, the same four temporal resolutions were adopted for the model simulations of  
190 this study.  
191



192  
193 Figure 1. Details of the NWFP sub-catchment selected for this study (sub-catchment number  
194 6 of 15, consisting of a single field called Golden Rove).

195

196 2.4 *Statistical analysis*

197 Two distinct sets of statistical analyses were conducted with respect to model performance  
198 and data resolution: (a) model performance for each of the four data temporal resolutions,  
199 separately (i.e. 15-minute measured versus 15-minute simulated; hourly measured versus  
200 hourly simulated; 6-hourly measured versus 6-hourly simulated; daily measured versus daily  
201 simulated); and (b) model performance conducted at the daily temporal resolution only,  
202 where 15-minute, hourly and 6-hourly simulations were each aggregated to the daily scale.  
203 The latter analyses provide valuable insights into the worth of using fine temporal resolution  
204 data to increase the accuracy of daily simulations, especially with respect to the accurate  
205 identification of extremes. This is important as many process-based models in the literature  
206 simulate only at a daily time-step (e.g. Del Grosso et al., 2009).

207

208 2.4.1 Model performance graphics

209 Model performance graphics consist of time-series plots, density plots and scatterplots of  
210 measured and simulated datasets. For the latter, the ideal 1:1 line, a linear regression fit, and a  
211 non-linear regression fit (i.e., a Loess smoother fit; Cleveland, 1979) are given where the  
212 estimated intercept and slope parameters from the linear fit should equal zero and one for  
213 perfect model simulations, respectively. Results ( $p$ -values) from a linear hypothesis test are  
214 reported comparing this ideal model with the estimated model using a finite sample  $F$  test  
215 (see Fox, 2016). The non-linear regression provides added insight into where the simulated  
216 values tend to over- or under-predict (e.g., at measured low or high values, respectively).  
217 Time-series plots for the errors (i.e. measured minus simulated data) are also given.

218

219 2.4.2 Model performance indices

220 To further assess the accuracy of the simulations, six accuracy indices were calculated: the  
 221 mean absolute error (MAE), the normalized root mean square error (NRMSE), the percentage  
 222 bias (PBIAS), the Nash-Sutcliffe efficiency (NSE), the index of agreement ( $d$ ) and the Kling-  
 223 Gupta efficiency (KGE), as given in Table 1.

224

225 Table 1. Accuracy indices formulae, where  $\hat{z}_i$  are the simulated values,  $z_i$  are the measured  
 226 values,  $\bar{z}_i$  is the mean of the measured values,  $r$  is the Pearson product-moment correlation  
 227 coefficient (between measured and simulated) and  $\sigma$  is the standard deviation.

Index form	Index formula	Min.	Max.	Ideal
Error	$MAE = \frac{1}{N} \sum_{i=1}^N  \hat{z}_i - z_i $	0	$\infty$	0
Error	$NRMSE = 100 \frac{\sqrt{\frac{1}{N} \sum_{i=1}^N (\hat{z}_i - z_i)^2}}{Z_{max} - Z_{min}}$	0	$\infty$	0
Error	$PBIAS = 100 \frac{\sum_{i=1}^N (\hat{z}_i - z_i)}{\sum_{i=1}^N z_i}$	0	$\infty$	0
Agreement	$NSE = 1 - \frac{\sum_{i=1}^N (\hat{z}_i - z_i)^2}{\sum_{i=1}^N (z_i - \bar{z}_i)^2}$	$-\infty$	1	1
Agreement	$d = 1 - \frac{\sum_{i=1}^N (\hat{z}_i - z_i)^2}{\sum_{i=1}^N ( \hat{z}_i - \bar{z}_i  +  z_i - \bar{z}_i )^2}$	0	1	1

Agreement	$KGE = 1 - \sqrt{(r - 1)^2 + \left(\frac{\sigma_z}{\sigma_z} - 1\right)^2 + \left(\frac{\bar{z}}{\bar{z}} - 1\right)^2}$	$-\infty$	1	1
-----------	--	-----------	---	---

228

### 229 2.4.3 Simulation accuracy of measured peaks

230 To investigate model accuracy in simulating water flux peaks, a threshold at the 99<sup>th</sup>  
 231 percentile of each measured water flux dataset was used to identify peak flows. Model  
 232 simulations were then assessed to determine if they could similarly exceed this threshold  
 233 coinciding with a measured exceedance. Incidences of correct peak flow simulations, false  
 234 negatives (simulation does not exceed threshold when measured flow does), false positives  
 235 (simulation exceeds threshold when measured flow does not) and corresponding Kappa  
 236 values are reported. The Kappa statistic provides a measure of agreement beyond the level of  
 237 agreement expected by chance alone. General guidelines for Kappa values are as follows: less  
 238 than 0.2 slight agreement, 0.2 to 0.4 fair agreement, 0.4 to 0.6 moderate agreement, 0.6 to 0.8  
 239 substantial agreement, greater than 0.8 almost perfect agreement, and equal to 1 perfect  
 240 agreement.

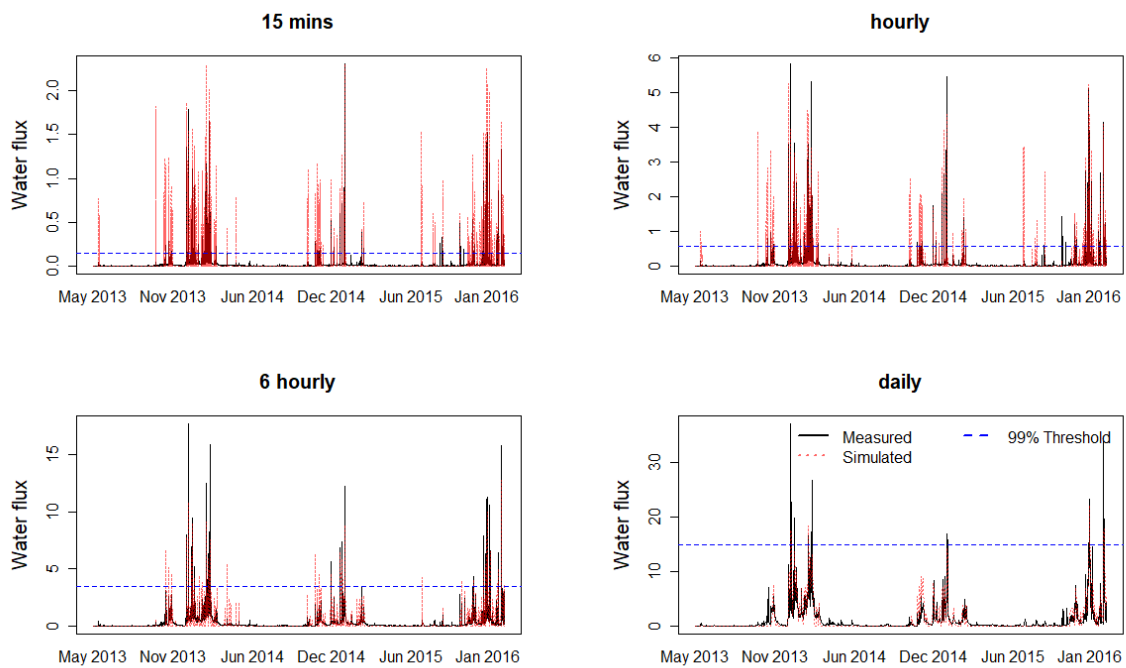
241

## 242 3 Results

### 243 3.1 Model performance for each of the four data temporal resolutions, separately

244 Comparisons between the measured and simulated water flux rates at different temporal  
 245 resolutions are shown in Fig. Figure 2. Visually, it appears that simulations of daily and 6-  
 246 hourly water fluxes tend to under-predict the measured data, often missing high peaks, while  
 247 simulations of 15-minute and hourly data possibly tend to over-predict. However, the  
 248 scatterplots of the measured and simulated data, together with the ideal 1:1 line, a linear

249 regression fit, and a Loess smoother fit (Fig. Figure 3) present a more complete picture.  
 250 Simulations for all four temporal resolutions clearly tend to over-predict, with the level of  
 251 over-prediction increasing as the resolution increases. Over-prediction is shown with each  
 252 linear regression fit lying below the 1:1 line; and increasingly so, as the resolution increases.  
 253 All linear regression fits were found to be significantly different to the 1:1 line, each with  $F$ -  
 254 test  $p$ -values  $< 0.0001$ .



255

256

257 Figure 2. Time-series plots for measured and simulated water flux data (not aggregated) for  
 258 15-minute, hourly, 6-hourly and daily data (in units of  $\text{mm } 15\text{min}^{-1}$ ,  $\text{mm h}^{-1}$ ,  $\text{mm } 6\text{h}^{-1}$  and  $\text{mm}$   
 259  $\text{d}^{-1}$ , respectively). All plots are shown with a threshold at the 99th percentile of measured data  
 260 (at  $0.138 \text{ mm } 15\text{min}^{-1}$ ,  $0.553 \text{ mm h}^{-1}$ ,  $3.45 \text{ mm } 6\text{h}^{-1}$  and  $14.9 \text{ mm d}^{-1}$ , respectively).

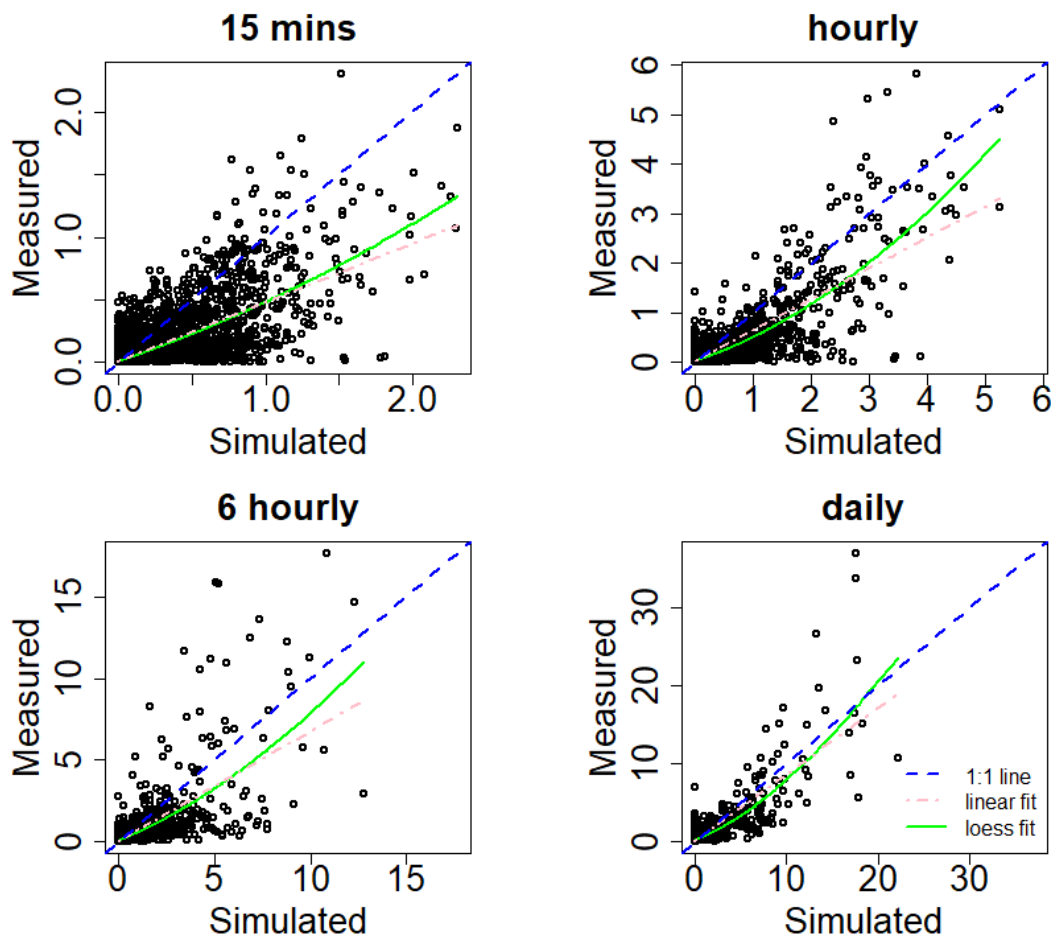
261

262 For all four temporal resolutions, the tendency to over-predict decreases at the largest

263 measured water fluxes, as shown by the concave behaviour of the loess smoother fit (Fig.

264 Figure 3), with daily simulations tending to under-predict at very large fluxes, thus, missing  
265 extreme events that may cause flooding and associated nutrient and sediment losses. Clearly,  
266 ‘smoothing bias’ increases as temporal resolution decreases. The 15-minute simulations  
267 maintain the variation shown in the measured data (i.e. observations range from 0 to 2.306  
268 mm 15min<sup>-1</sup> while simulations range from 0 to 2.310 mm 15min<sup>-1</sup>), while the daily  
269 simulations do not (i.e. observations range from 0 to 36.97 mm d<sup>-1</sup> while simulations only  
270 range from 0 to 22.20 mm d<sup>-1</sup>). As each ‘simulation-to-observation’ comparison is on a  
271 different scale, it is not useful to present further model fit diagnostics, such as error and  
272 agreement indices.

273



275 Figure 3. Scatterplots of the measured and simulated data (not aggregated) for 15-minute,  
276 hourly, 6-hourly and daily data. Scatterplots are shown with the 1:1 line, a linear regression  
277 fit and a loess smoother fit. Units are in  $\text{mm } 15\text{min}^{-1}$ ,  $\text{mm h}^{-1}$ ,  $\text{mm } 6\text{h}^{-1}$  and  $\text{mm d}^{-1}$ ,  
278 respectively.

279

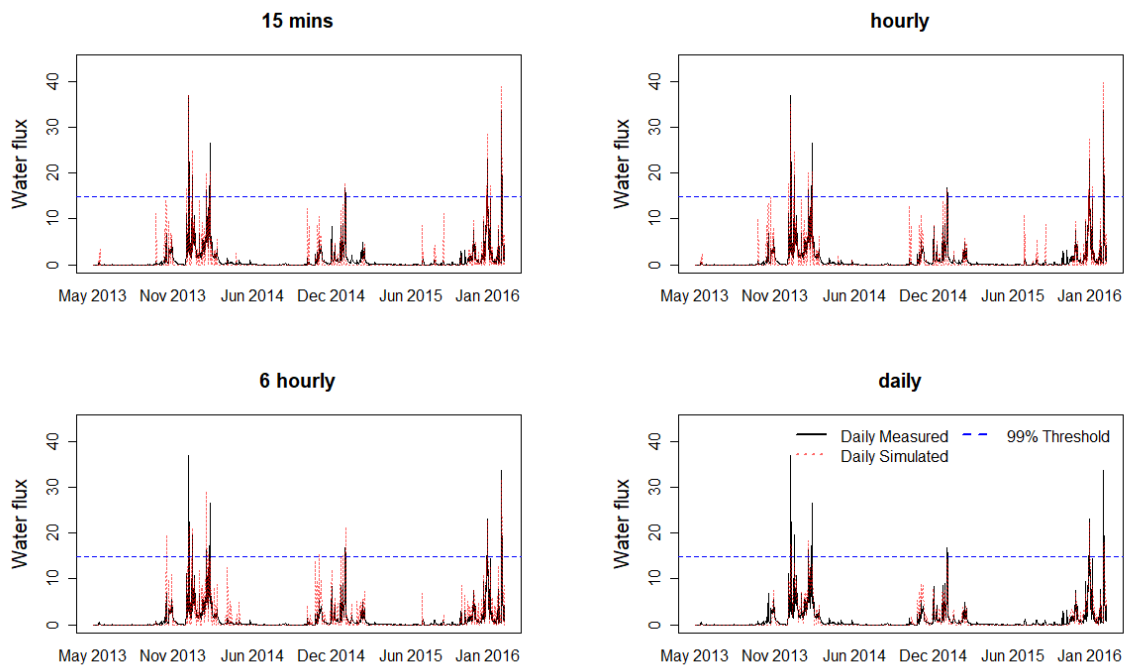
### 280 3.2 *Model performance for simulations aggregated to the daily scale*

281 Comparisons between the measured and simulated water flux rates aggregated to the same  
282 daily scale are shown in Fig. Figure 4. There are clear instances of both over- and under-  
283 prediction for all four daily outputs. The scatterplots (Fig. Figure 5) of daily measured and  
284 daily simulated data from different aggregations, together with the 1:1 line, a linear fit, and a  
285 loess smoother fit, again provide a clear visualisation of the relations in the time-series plots.  
286 Simulations for all three aggregations to daily (15-minute, hourly and 6-hourly) again tend to  
287 over-predict (as their linear fits lie below the 1:1 line), but this over-prediction is broadly  
288 similar across the four datasets, and not as great as that found with the unaggregated data,  
289 above. The 6-hourly aggregations appear to be the least accurate. Again, all linear regression  
290 fits were found to be significantly different to the 1:1 line, each with  $F$ -test  $p$ -values  $<$   
291 0.0001.

292

293 In this instance, ‘smoothing boas’ increases as aggregation resolution decreases, where  
294 simulations for 15-minute and hourly aggregations both increase the variation shown in the  
295 measured daily data (i.e. 0 to  $36.97 \text{ mm d}^{-1}$ ); with 15-minute daily aggregations ranging from  
296 0 to  $38.94 \text{ mm d}^{-1}$  and hourly daily aggregations ranging from 0 to  $39.64 \text{ mm d}^{-1}$ . Conversely,  
297 the 6-hourly daily aggregations and the daily simulations reduce variation with the 6-hourly  
298 daily aggregations ranging from 0 to  $31.70 \text{ mm d}^{-1}$  and the (unaggregated) daily simulations

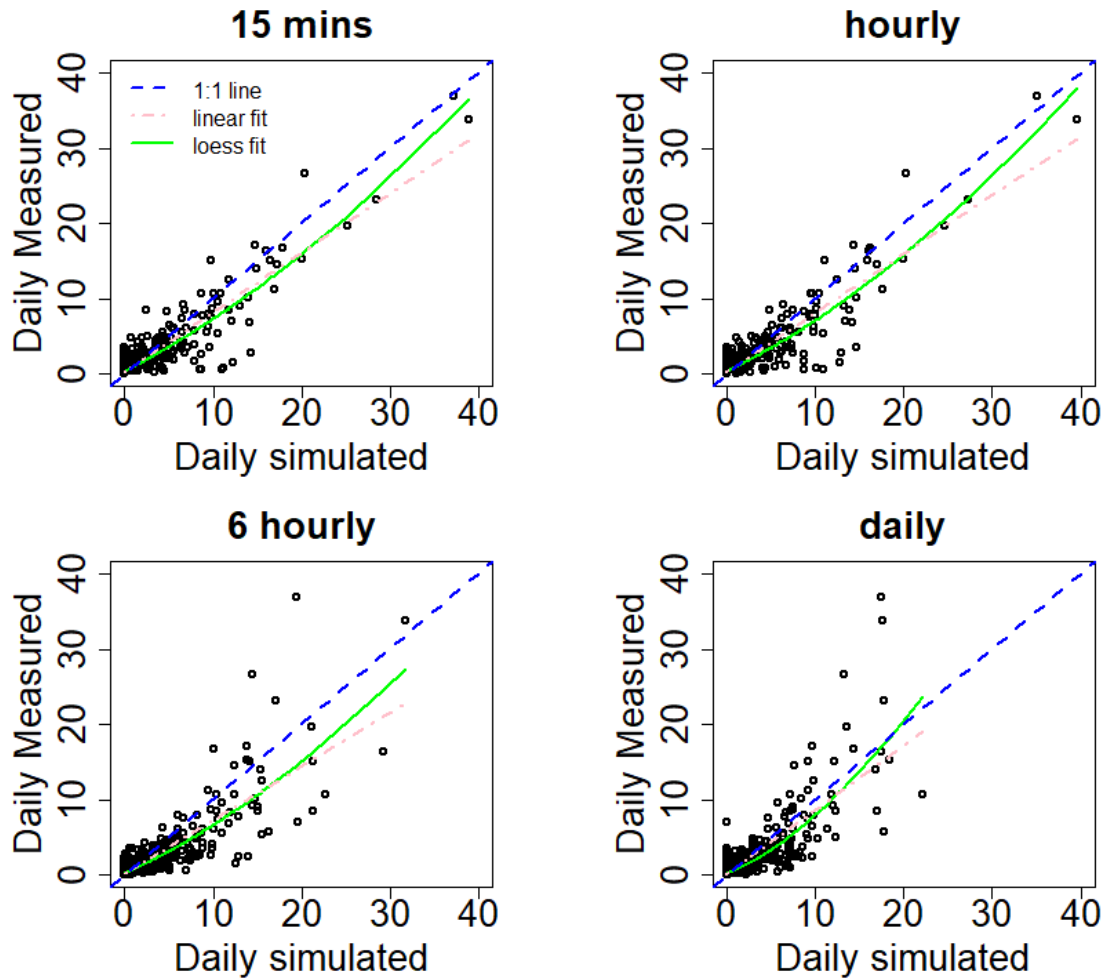
299 ranging from 0 to 22.20 mm d<sup>-1</sup>. In summary, daily simulations based on component 15-  
300 minute and hourly aggregations have the potential to identify peak water fluxes (and, thus,  
301 flood events) and predict their magnitudes more accurately, relative to 6-hourly aggregations  
302 and (unaggregated) daily simulations.



303

304 Figure 4. Time-series plots for daily measured and daily simulated water flux data (with the  
305 first three plots having data aggregated from: 15 minutes to daily; hourly to daily; 6 hourly to  
306 daily). All units in mm d<sup>-1</sup>. All plots are shown with a threshold at the 99th percentile of  
307 measured data (14.90 mm d<sup>-1</sup>).

308



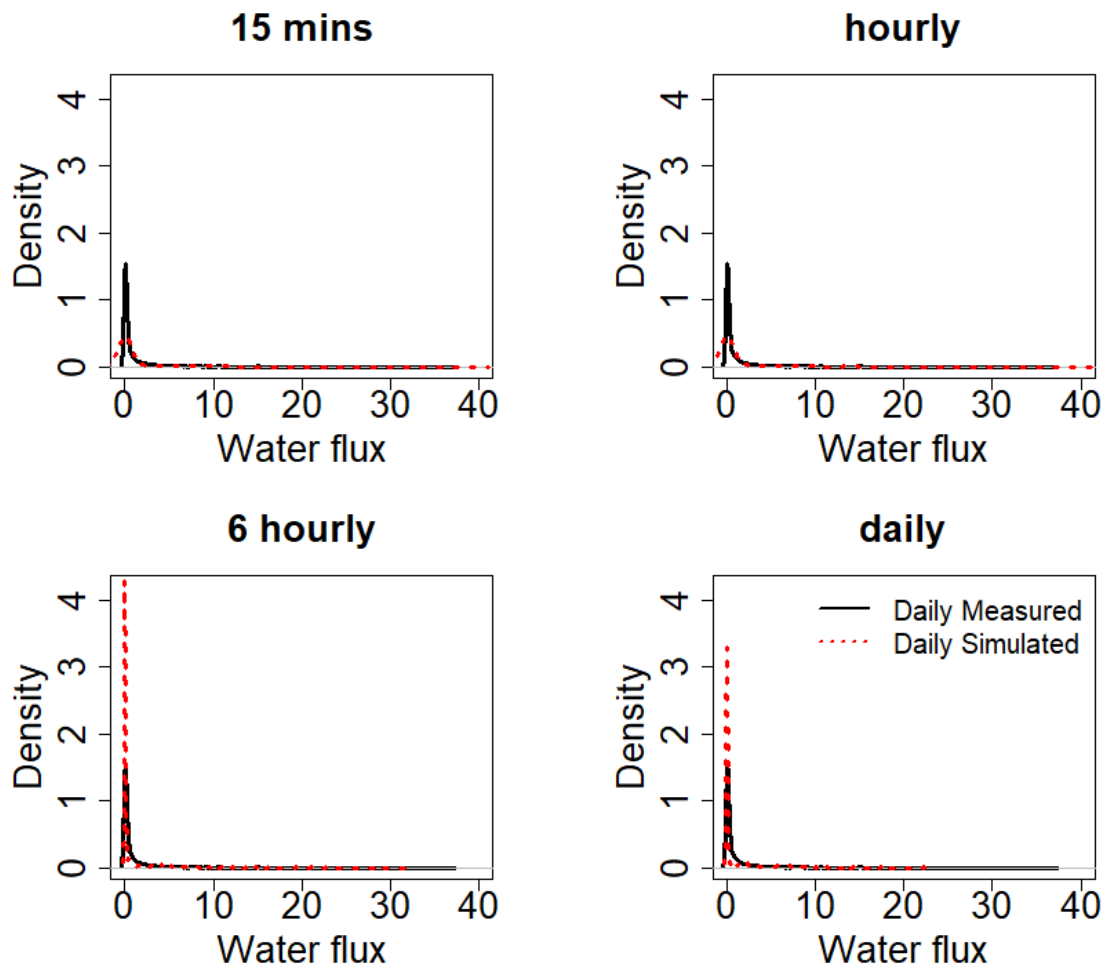
309

310 Figure 5. Scatterplots of the daily measured and daily simulated water flux (with the first  
 311 three plots having data aggregated from: 15 minutes to daily; hourly to daily; 6 hourly to  
 312 daily). Scatterplots are shown with the ideal 1:1 line, a linear regression fit and a loess  
 313 smoother fit. All units in  $\text{mm d}^{-1}$ .

314

315 Further clarity on bias is provided in the density plots for the measured and simulated data  
 316 (Fig. Figure 6). Here, daily simulations based on 15-minute and hourly aggregations have a  
 317 lower density at small daily water fluxes than that found with the measured data, while the 6-  
 318 hourly aggregations and (unaggregated) daily simulations have a higher density at small daily  
 319 water fluxes. This is combined with a longer tail in the density curve for the 15-minute and

320 hourly aggregations, as each can simulate large daily water fluxes, while the 6-hourly  
321 aggregation and (unaggregated) daily simulations do not have this property.



322

323

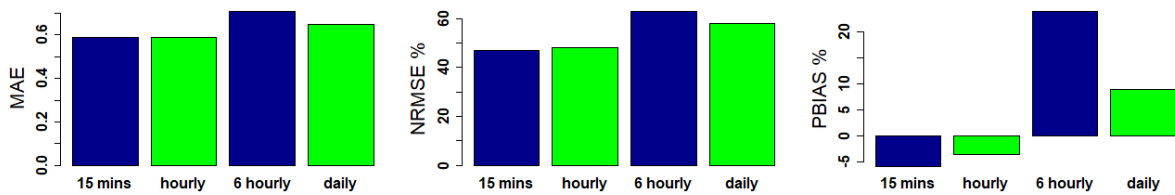
324 Figure 6. Density plots for daily measured and daily simulated data (with the first three plots  
325 having data aggregated from: 15 minutes to daily; hourly to daily; 6 hourly to daily). All units  
326 in  $\text{mm d}^{-1}$ .

327

328 The error indices (MAE, NRMSE and PBIAS) are reported for each daily aggregation in Fig.  
329 Figure 7, where the 15-minute and hourly aggregations clearly perform more accurately than  
330 the 6-hourly aggregation and (unaggregated) daily simulations. Errors (i.e. residuals) are also

331 reported over the study time period in Fig. Figure 8, where errors tend to be larger for the  
 332 daily simulations based on the 6-hourly aggregation and the (unaggregated) daily simulations.  
 333 Interestingly, the 6-hourly aggregation consistently is the least accurate, including being less  
 334 accurate than the (unaggregated) daily simulations.

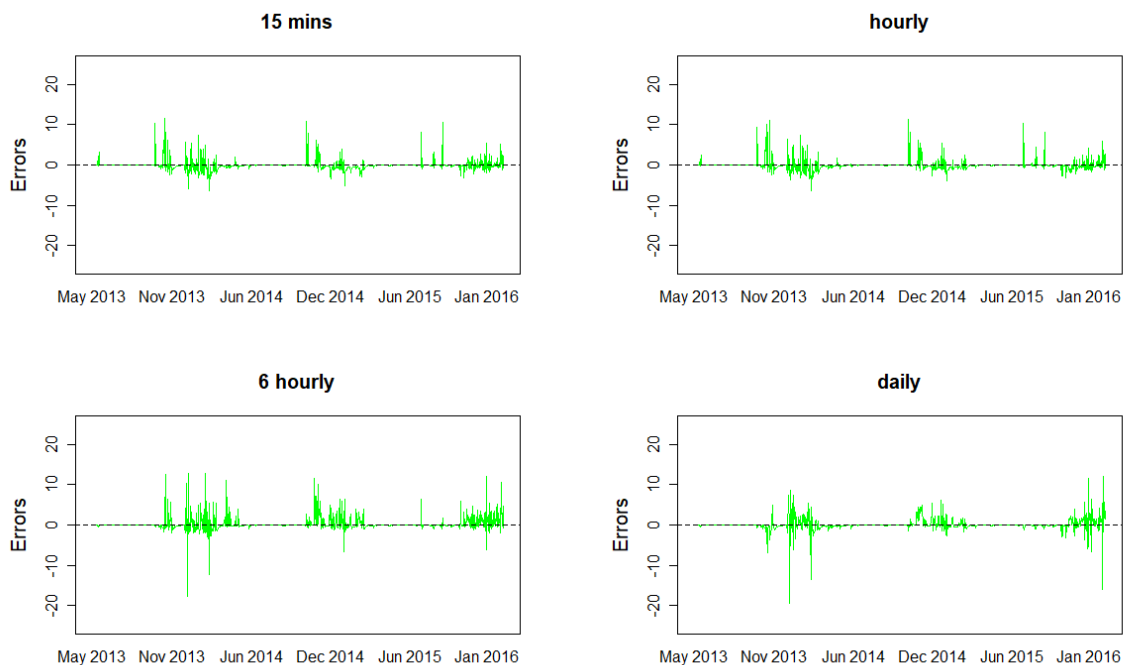
335



336

337 Figure 7. Error (MAE, NRMSE, PBIAS) indices with respect to daily measured and daily  
 338 simulated data (with 15-minute, hourly, 6-hourly data aggregated to daily).

339



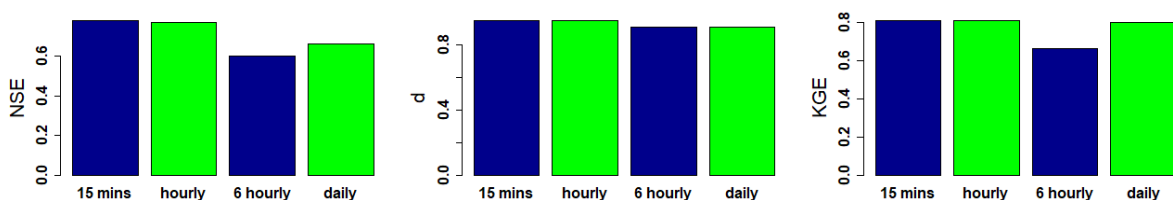
340

341 Figure 8. Time-series of errors (simulated minus measured data) aggregated to the daily  
342 temporal resolution. All units in  $\text{mm d}^{-1}$ . Positive errors represent over-prediction by the  
343 model.

344

345 Agreement indices (NSE,  $d$  and KGE) are reported for each daily aggregation in Fig. Figure  
346 9, where again the 15-minute and hourly aggregations perform more accurately than the 6-  
347 hourly aggregation and (unaggregated) daily simulations (although daily simulations perform  
348 relatively well according to the KGE index). From the given accuracy diagnostics, it is not  
349 immediately apparent whether daily simulations based on 15-minute or hourly aggregations  
350 are the most accurate, and as such, both appear to increase the accuracy relative to  
351 SPACSYS' daily simulations. Again, the 6-hourly aggregation is the least accurate.

352



353

354 Figure 9. Agreement (NSE,  $d$ , KGE) indices with respect to daily measured and daily  
355 simulated data (with 15-minute, hourly, 6-hourly simulations aggregated to daily).

356

### 357 3.3 Simulation of measured peaks

358 To investigate the ability of the model to simulate and identify water flux peaks, the 99<sup>th</sup>  
359 percentile of each measured water flux dataset was used as a threshold to identify peak flows,  
360 as highlighted in Figs. Figure 2 and Figure 4 (the dashed blue line). Incidences of correct

361 peak flow simulations, false negatives, false positives and the resultant Kappa values are  
362 given in Table 2. It appears that hourly simulations provide the largest correct classification  
363 rate (Kappa = 0.553) for the unaggregated approach, but with only moderate success in  
364 identifying measured peak flows (as a promising 92% identification rate is tempered by a  
365 poor mis-identification rate). Conversely, aggregating to the daily scale using either 15-  
366 minute or hourly simulations was able to provide much greater agreement in identifying  
367 measured peak flows at the daily scale, with each identifying 9 out of 11 peak flow events  
368 correctly, coupled with only 2 false positives (Kappa = 0.816 in both cases). This level of  
369 agreement was far greater than that found through directly simulating the daily data, which  
370 provided only moderate success in identifying measured peak flows (Kappa = 0.495). Again,  
371 the 6-hourly aggregation is the least accurate with a relatively high number of false positives  
372 (simulated flow exceeds the threshold when measured flow does not).

373

374 Table 2. Accuracy at peak water fluxes according to simulation resolution. Peaks taken at 99<sup>th</sup>  
375 percentile of measured data (see the dashed blue line in Figs. Figure 2 and Figure 4).

<b>Simulation resolution</b>	<b>Sample size</b>	<b>Measured Peaks</b>	<b>Correctly Simulated</b>	<b>False Negative</b>	<b>False Positive</b>	<b>Kappa</b>
<b>Unaggregated</b>						
15-minute	97920	980	759 (77)*	221	1224	0.506
hourly	24480	245	225 (92)	20	335	0.553
6-hourly	4080	41	32 (78)	9	52	0.503
daily	1020	11	5 (45)	6	4	0.495
<b>Aggregated to daily</b>						
15-minute	1020	11	9 (82)	2	2	0.816

hourly	1020	11	9 (82)	2	2	0.816
6-hourly	1020	11	6 (55)	5	9	0.455
daily	1020	11	5 (45)	6	4	0.495

376 \* Value in brackets shows a percentage of correctly simulated peaks to measured peaks.

## 377 **4 Discussion**

### 378 *4.1 Model performance*

#### 379 4.1.1 Unaggregated data

380 The statistical analyses for model performance suggested that the SPACSYS model simulates  
381 the general trend of water fluxes at the four different temporal resolutions reasonably well  
382 (Figs. Figure 2 and Figure 3). All simulations tended to over-predict water flux, however, and  
383 only simulations at the finest resolutions maintained the variation in the measured data. The  
384 accuracy of water flux peak simulations varied among the four resolutions (Table 2). Almost  
385 92% of the measured peaks over the simulated period were modelled correctly at an hourly  
386 resolution, the resolution with the smallest misclassification rate. However, this was tempered  
387 by a high rate of predicting peaks that did not exist. A previous statistical analysis of peak  
388 flows at different scales from a different NWFP sub-catchment (similar in size to the one  
389 used here), modelled and simulated by a Generalized Pareto distribution, also showed the  
390 greatest agreement at the hourly resolution (Curceac et al., 2020).

391

#### 392 4.1.2 Aggregated to Daily

393 When simulations at a finer temporal resolution were aggregated to a daily rate, the  
394 simulation results using both the 15-minute and hourly aggregations showed the greatest  
395 accuracy broadly equally, both in the prediction of general trends (Figs. Figure 4 to Figure 9)

396 and the identification of peak flows (Table 2). This demonstrates clearly that the daily  
397 simulation of water fluxes with the SPACSYS model, informed by finer temporal resolution  
398 data, can increase simulation accuracy. This result is an important advance relative to  
399 previous SPACSYS studies, which only used a daily time-step, and which similarly used sub-  
400 catchments of the NWFP as the study site (Liu et al., 2018).

401 The simulation results using both the 15-minute and hourly aggregations showed the greatest  
402 accuracy broadly equally. When the simulation time step is getting longer, average  
403 precipitation intensity might be weaker, which causes simulated water fluxes smoother and  
404 the deviations with monitored water fluxes larger. Given the complexity of the soil-water  
405 processes that operate across the field, it is not surprising to see substantial variation around  
406 the 1-1 line when predicting flow at 15-minute to 6-hour scales due to inherent variability.  
407 We would expect to see a similar phenomenon with any similar process-based model. What  
408 is important is that when these fine-scale predictions are aggregated we get substantial  
409 improvements to daily predictions.

#### 410 *4.2 Results in context and their generalisation*

411 Results are consistent with other studies that similarly showed that differences in the  
412 (unaggregated or aggregated) time-step have the greatest impact on runoff simulation  
413 accuracy relative to other factors, some of which, also investigated changes in spatial  
414 resolution (i.e. aggregating over different spatial units) (Choi et al., 2018; Huang et al., 2019;  
415 Jeong et al., 2010; Kavetski et al., 2011; Merz et al., 2009). Thus, the value of using  
416 aggregated fine temporal resolution simulations to increase the accuracy of daily simulations  
417 can be said to hold generally for other process-based models provided the hydrological  
418 process is described appropriately. However, it does not follow that daily simulation accuracy  
419 will continue to increase as the temporal resolution of the aggregated data becomes finer.  
420 This study found aggregating hourly simulations to daily to be just as accurate as aggregating

421 15-minute simulations to daily, while aggregating 6-hourly simulations to daily performed  
422 less well than the usual daily simulations.

423

424 The temporal resolution for process-based models should be chosen carefully to balance  
425 between capturing all important processes, the study objectives and data availability. For our  
426 study, with flooding as context, the identification of water flux extremes in a grassland field  
427 (or small sub-catchment) with a heavy clayed soil, is viewed as *the* important process, more  
428 so than capturing broad trends in water flux. It is well-known that running a model at a finer  
429 resolution, then aggregate, will increase the prediction accuracy in a broad sense (see above).  
430 What has received less attention in the literature is the effects of temporal resolution on a  
431 model's ability to capture extremes (e.g. see Schaller et al., 2020, in the context of  
432 streamflow). In this respect, our study has found daily peak flows to be more accurately  
433 identified using aggregations of simulations at finer resolutions, than using coarse daily  
434 simulations directly. Of course, measurement at a finer resolution comes at a cost and this  
435 needs to be balanced with associated improvements in model accuracy. In this instance, this  
436 interplay is simple to resolve since aggregating to the daily scale using both 15-minute and  
437 hourly simulations were equally as accurate, meaning measuring at an hourly interval would  
438 be sufficient for the case study site.

439

440 The appropriate temporal resolution to simulate water fluxes using a hydrological model  
441 depends on hydro-climatological and geophysical characteristics, and the scale of the process.  
442 It has been suggested that an appropriate temporal resolution could be between 12 hours for  
443 middle-sized upstream areas and 48 hours for a complete river basin (Booij and Tran, 2005).  
444 As the size of the field for this study is  $< 4$  ha, the indicated hourly resolution appears

445 reasonable. Observed and projected changes in the UK's climate suggest an increase in heavy  
446 rain events and wetter winters (Committee on Climate Change, 2017), where some UK  
447 regions will be more affected than others. This will inevitably change agricultural  
448 management practice and land use across the UK. Taking as an example the grazed pasture of  
449 this study, introducing a deep-rooting grass suited to its heavy clay soils (Macleod et al.,  
450 2013) and/or the mechanical loosening of topsoil (Newell-Price et al., 2011) would reduce  
451 water runoff, whereas conversion to an arable crop (e.g. wheat) would provide its own set of  
452 water runoff influences. Such changes would alter the characteristics of the water fluxes  
453 generated, as the field's soil properties will change, meaning the determination of an  
454 appropriate resolution to simulate water fluxes may also change from the hourly resolution  
455 suggested here. This is analogous to other hydrological studies where, for example, different  
456 overflow designs in roof drainage structures have markedly variable responses to rainfall  
457 intensity increases (Verstraten et al., 2019).

458

#### 459 *4.3 Inputs that impact hydrological model performance*

460 Key model input variables such as precipitation can determine the impacts of simulation  
461 time-steps on the performance of hydrological models; for example, the duration and  
462 temporal variability of a precipitation event in relation to the rainfall–runoff lag time (Ficchi  
463 et al., 2016). A multiple-day precipitation event is the main cause of continuous runoff events  
464 and related peaks. For example, for this study, there was almost an unbroken measured  
465 precipitation period from 14 December 2013 to 5 March 2014, which brought a total of 541  
466 mm of precipitation, 78% of which was measured as surface runoff (i.e., measured water  
467 flux). Study simulations showed 70, 70, 81 and 85% as water fluxes over the period at the 15-  
468 minute, hourly, 6-hourly and daily resolutions, respectively. Previous studies showed that  
469 wetter soils had less capacity to store water, resulting in greater runoff volumes (Huang et al.,

470 2017; Kibet et al., 2014; Zehe et al., 2010). Both observations and simulations in this study  
471 confirmed this finding. Conversely, for a single day event, a measured 92% of 40.2 mm daily  
472 precipitation was discharged on 23 December 2013. The simulations generated 99, 99, 90 and  
473 44% water losses at the 15-minute, hourly, 6-hourly and daily resolutions, respectively. Thus,  
474 almost all of the precipitation contributed to the water loss on this day, where only the daily-  
475 scale simulation did not capture this. However, although heavy rainfall is necessary to  
476 generate water fluxes, it is not a sufficient condition for a higher surface runoff rate to occur  
477 (Ledingham et al., 2019). For example, there was about 25 mm precipitation on 14 May 2013  
478 and on 13 August 2015, but both the simulations and the observations (at all four resolutions)  
479 did not show apparent water fluxes. Further, a daily precipitation of 4 mm on 27 February  
480 2015 generated a measured 120% water loss, together with simulated values of 48, 148, 125  
481 and 75% water loss at the 15-minute, hourly, 6-hourly and daily resolutions, respectively.

482

483 The generation of water fluxes not only depends on the intensity of precipitation, but also  
484 surface coverage, topology and soil physical properties of the field. In hydrology, lag time,  
485 defined as the time difference between the peak runoff and mass centre of rainfall excess  
486 (Hall, 1984), is usually used to determine a runoff rate. Although the SPACSYS model does  
487 not use this parameter to estimate the surface runoff rate, it uses the Richard's equation to  
488 calculate soil water redistribution where soil hydraulic conductivity, saturated water content  
489 and plant uptake play critical roles in water infiltration and consequently surface runoff. A  
490 trial study on the spatial variation of soil hydraulic conductivity (unpublished data) in a  
491 NWFP field, nearby to the study field, highlighted clear within-field variation, partially  
492 because of compaction caused by grazed animal movement. However, the soil physical  
493 properties used in the simulations were estimated based on soil texture, and at the field-scale  
494 only. The error and uncertainty introduced by this approach are likely to be transferred to the

495 errors in simulating infiltration and surface runoff rates. To improve model simulation  
496 accuracy, soil physical properties as core information should be provided wherever possible.

497

#### 498 *4.4 Further considerations of scale*

499 The processes controlling water fluxes operate across a range of spatial and temporal scales,  
500 and the time-series that are recorded represent an aggregation of these effects. For example,  
501 effects of evapotranspiration will dominate at annual scales whereas more local impacts of  
502 precipitation will manifest at finer scales (Rust et al., 2014). As noted above, the  
503 characteristics of the study area, (e.g. size, soil condition and topography) will impact the  
504 dominant scales of variation and hence the frequency at which it is most appropriate to model  
505 or measure water fluxes. Rust et al. (2014) presented an analysis which aimed to determine  
506 whether the process-based model they studied captured the scale-dependent variation  
507 measured in catchment runoff. They analysed model residuals using wavelet-based signal  
508 processing methods and found that although their model captured broadly the scale-  
509 dependent variation in the data, fine scale variation was always under-predicted. Our results  
510 shed light on their observation as we confirm that if the scale of the model prediction is not  
511 sufficiently fine then model-damping will result in an under-prediction of extreme events.

512

## 513 **5 Conclusions**

514 For the grassland study site, the adapted process-based model (SPACSYS) could adequately  
515 simulate the trends in measured water fluxes and identify their extremes. At a daily time-step,  
516 model accuracy increased when simulations were run at finer temporal resolutions,  
517 specifically 15-minute and hourly, and then aggregated to daily (a coarse output resolution

518 commonly used in field-scale agricultural settings). Aggregating using 6-hourly simulations  
519 was less accurate. For the study site, which constitutes a field of a grassland research farm  
520 platform (NWFP), simulation of water fluxes at an hourly resolution is likely optimal since  
521 use of the 15-minute resolution did not increase prediction accuracy or the ability to identify  
522 extremes in flow further. Therefore, for modelling purposes, monitoring frequency could be  
523 reduced safely to hourly from the current 15-minute resolution.

524

525 Results provide information not only for the NWFP experiment, but also and indirectly, the  
526 UK grassland farming regions that its outputs upscale to (Pulley and Collins, 2019). Study  
527 results are crucial in relation to meeting the increasing demand for reliable simulation-based  
528 runoff forecasts at daily and sub-daily resolutions, where accurate knowledge of peak  
529 discharge and stage are essential not only for flood protection, but also to help increase the  
530 forecast accuracy of associated emissions such as nutrient or sediment loss, that each use  
531 water flux as a component. Further research is called for in specifying the temporal resolution  
532 amongst the wide range of field-scale hydrological/agricultural models currently applied.  
533 This needs to be coupled with linked changes in climate and land use to increase model  
534 forecast accuracy and to optimise data acquisition schemes on farms generally.

535

## 536 **6 Acknowledgements**

537 This research was funded by the BBSRC Institute Strategic Programme grant, “Soils to  
538 Nutrition” (BBS/E/C/000I0330, BBS/E/C/000I0320), the BBSRC National Capability grant  
539 for the North Wyke Farm Platform (BBS/E/C/000J0100) and a PhD studentship funded by  
540 Rothamsted Research and Lancaster University.

541

## References

542

543 Abalos, D., Cardenas, L.M., Wu, L., 2016. Climate change and N<sub>2</sub>O emissions from South  
544 West England grasslands: a modelling approach. *Atmos. Environ.*, 132: 249-257.  
545 DOI:<https://doi.org/10.1016/j.atmosenv.2016.03.007>

546 Adimassu, Z., Alemu, G., Tamene, L., 2019. Effects of tillage and crop residue management  
547 on runoff, soil loss and crop yield in the Humid Highlands of Ethiopia. *Agric. Syst.*, 168:  
548 11-18. DOI:<https://doi.org/10.1016/j.agsy.2018.10.007>

549 Ahuja, L.R., Ma, L., Howell, T.A., 2002. *Agricultural System Models in Field Research and*  
550 *Technology Transfer*. CRC Press, Boca Raton.

551 Alaoui, A., Rogger, M., Peth, S., Blöschl, G., 2018. Does soil compaction increase floods? A  
552 review. *J. Hydrol.*, 557: 631-642. DOI:<https://doi.org/10.1016/j.jhydrol.2017.12.052>

553 Archer, D.R., Fowler, H.J., 2018. Characterising flash flood response to intense rainfall and  
554 impacts using historical information and gauged data in Britain. *J. Flood Risk Manag.*,  
555 11: S121-S133. DOI: <https://doi.org/10.1111/jfr3.12187>

556 Bingham, I.J., Wu, L., 2011. Simulation of wheat growth using the 3D root architecture model  
557 SPACSYS: validation and sensitivity analysis. *Eur. J. Agron.*, 34: 181-189.  
558 DOI:<https://doi.org/10.1016/j.eja.2011.01.003>

559 Booij, M.J., Tran, H.M., 2005. Appropriate scales for hydro-climatological variables in the Red  
560 River basin. In: Wagener, T. et al. (Eds.), *Proceedings of symposium S6 held during*  
561 *the Seventh IAHS Scientific Assembly*. IAHS publication. IAHS Press, pp. 325-332.

562 Brown, I., Thompson, D., Bardgett, R., Berry, P., Crute, I., Morison, J., Morecroft, M., Pinnegar,  
563 J., Reeder, T., Topp, K., 2016. *UK Climate Change Risk Assessment Evidence Report:*  
564 *Chapter 3, Natural Environment and Natural Assets*. Report Prepared for the  
565 *Adaptation Sub-committee of the Committee on Climate Change*, London.

566 Carswell, A.M., Gongadze, K., Misselbrook, T.H., Wu, L., 2019. Impact of transition from  
567 permanent pasture to new swards on the nitrogen use efficiency, nitrogen and carbon  
568 budgets of beef and sheep production. *Agric. Ecosyst. Environ.*, 283: 106572.  
569 DOI:<https://doi.org/10.1016/j.agee.2019.106572>

570 Charlton, M.B., Bailey, A., Arnell, N., 2010. *Water for Agriculture – Implications for Future*  
571 *Policy and Practice Report for the Royal Agricultural Society of England*.

572 Choi, Y.S., Shin, M.-J., Kim, K.T., 2018. Preliminary study of computational time steps in a  
573 physically based distributed rainfall–runoff model. *Water*, 10: 1269. DOI:  
574 <https://doi.org/10.3390/w10091269>

575 Cleveland, W.S., 1979. Robust locally weighted regression and smoothing scatterplots. *J. Am.*  
576 *Stat. Assoc.*, 74: 829-836. DOI:<https://10.1080/01621459.1979.10481038>

577 Committee on Climate Change, 2017. *UK Climate Change Risk Assessment 2017. Synthesis*  
578 *Report*, London.

579 Curceac, S., Atkinson, P.M., Milne, A., Wu, L., Harris, P., 2020. An evaluation of automated  
580 GPD threshold selection methods for hydrological extremes across different scales. *J.*  
581 *Hydrol.*, 585: 124845. DOI:<https://doi.org/10.1016/j.jhydrol.2020.124845>

582 Dadson, S.J., Hall, J.W., Murgatroyd, A., Acreman, M., Bates, P., Beven, K., Heathwaite, L.,  
583 Holden, J., Holman, I.P., Lane, S.N., O'Connell, E., Penning-Rowsell, E., Reynard, N.,  
584 Sear, D., Thorne, C., Wilby, R., 2017. A restatement of the natural science evidence  
585 concerning catchment-based 'natural' flood management in the UK. *Proc. R. Soc. A*,  
586 473: 20160706. DOI:<https://doi.org/10.1098/rspa.2016.0706>

587 Del Grosso, S.J., Ojima, D.S., Parton, W.J., Stehfest, E., Heistemann, M., DeAngelo, B., Rose,

588 S., 2009. Global scale DAYCENT model analysis of greenhouse gas emissions and  
589 mitigation strategies for cropped soils. *Glob. Planet. Change*, 67: 44-50.  
590 DOI:<https://doi.org/10.1016/j.gloplacha.2008.12.006>

591 Department for Environment, Food and Rural Affairs, 2019. *Agriculture in the United Kingdom*  
592 2018, London.

593 Environment Agency, 2009. *Flooding in England: A National Assessment of Flood Risk*, Bristol,  
594 UK.

595 Ficchi, A., Perrin, C., Andréassian, V., 2016. Impact of temporal resolution of inputs on  
596 hydrological model performance: An analysis based on 2400 flood events. *J. Hydrol.*,  
597 538: 454-470. DOI:<https://doi.org/10.1016/j.jhydrol.2016.04.016>

598 Fox, J., 2016. *Applied Regression Analysis and Generalized Linear Models (Third Edition)*.  
599 SAGE Publications Inc., California.

600 Hall, M.J., 1984. *Urban Hydrology*. Elsevier Applied Science Publishers, London.

601 Harrod, T.R., Hogan, D.V., 2008. *The soils of North Wyke and Rowden*, North Wyke Research,  
602 North Wyke, Devon.

603 Huang, J., Kang, Q., Yang, J.X., Jin, P.W., 2017. Multifactor analysis and simulation of the  
604 surface runoff and soil infiltration at different slope gradients. *IOP Conf. Ser. Earth*  
605 *Environ. Sci.*, 82: 012019. DOI:<https://doi.org/10.1088/1755-1315/82/1/012019>

606 Huang, Y., Bárdossy, A., Zhang, K., 2019. Sensitivity of hydrological models to temporal and  
607 spatial resolutions of rainfall data. *Hydrol. Earth Syst. Sc.*, 23: 2647-2663.  
608 DOI:<https://doi.org/10.5194/hess-23-2647-2019>

609 Jansson, P.-E., 1998. Simulation model for soil water and heat conditions. Description of the  
610 SOIL model. Division of Agricultural Hydraulics Communications 98:2, Swedish  
611 University of Agricultural Sciences, Uppsala.

612 Jeong, J., Kannan, N., Arnold, J., Glick, R., Gosselink, L., Srinivasan, R., 2010. Development  
613 and integration of sub-hourly rainfall-runoff modeling capability within a watershed  
614 model. *Water Resour. Manag.*, 24: 4505-4527. DOI:<https://doi.org/10.1007/s11269-010-9670-4>

615

616 Kavetski, D., Fenicia, F., Clark, M.P., 2011. Impact of temporal data resolution on parameter  
617 inference and model identification in conceptual hydrological modeling: Insights from  
618 an experimental catchment. *Water Resour. Res.*, 47: W05501. DOI:  
619 <https://doi.org/10.1029/2010WR009525>

620 Keesstra, S., Nunes, J., Novara, A., Finger, D., Avelar, D., Kalantari, Z., Cerdà, A., 2018. The  
621 superior effect of nature based solutions in land management for enhancing  
622 ecosystem services. *Sci. Total Environ.*, 610-611: 997-1009.  
623 DOI:<https://doi.org/10.1016/j.scitotenv.2017.08.077>

624 Kibet, L.C., Saporito, L.S., Allen, A.L., May, E.B., Kleinman, P.J.A., Hashem, F.M., Bryant,  
625 R.B., 2014. A protocol for conducting rainfall simulation to study soil runoff. *J. Vis. Exp.*:  
626 e51664. DOI:<https://doi.org/10.3791/51664>

627 Ledingham, J., Archer, D., Lewis, E., Fowler, H., Kilsby, C., 2019. Contrasting seasonality of  
628 storm rainfall and flood runoff in the UK and some implications for rainfall-runoff  
629 methods of flood estimation. *Hydrol. Res.*, 50: 1309-1323.  
630 DOI:<https://doi.org/10.2166/nh.2019.040>

631 Liu, Y., Li, Y., Harris, P., Cardenas, L., Dunn, R.M., Sint, H., Murray, P., Lee, M., Wu, L., 2018.  
632 Modelling field scale spatial variation in water run-off, soil moisture, N<sub>2</sub>O emissions and  
633 herbage biomass of a grazed pasture using the SPACSYS model. *Geoderma*, 315:  
634 49-58. DOI:<https://doi.org/10.1016/j.geoderma.2017.11.029>

- 635 Liu, Y., Wu, L., Watson, C.A., Baddeley, J.A., Pan, X., Zhang, L., 2013. Modeling biological  
636 dinitrogen fixation of field pea with a process-based simulation model. *Agron. J.*, 105:  
637 670-678. DOI:<https://doi.org/10.2134/agronj2012.0412>
- 638 Macleod, C.J.A., Humphreys, M.W., Whalley, W.R., Turner, L., Binley, A., Watts, C.W., Skot,  
639 L., Joynes, A., Hawkins, S., King, I.P., O'Donovan, S., Haygarth, P.M., 2013. A novel  
640 grass hybrid to reduce flood generation in temperate regions. *Sci. Rep.*, 3: 1683.  
641 DOI:<https://doi.org/10.1038/srep01683>
- 642 Merz, B., Plate, E.J., 1997. An analysis of the effects of spatial variability of soil and soil  
643 moisture on runoff. *Water Resour. Res.*, 33: 2909-2922.  
644 DOI:<https://doi.org/10.1029/97WR02204>
- 645 Merz, R., Parajka, J., Blöschl, G., 2009. Scale effects in conceptual hydrological modeling.  
646 *Water Resour. Res.*, 45: W09405. DOI: <https://doi.org/10.1029/2009WR007872>
- 647 Morison, J.I.L., Matthews, R.B., 2016. Agriculture and forestry climate change impacts  
648 summary report. DOI:[https://nerc.ukri.org/research/partnerships/ride/lwec/report-  
649 cards/agriculture/](https://nerc.ukri.org/research/partnerships/ride/lwec/report-cards/agriculture/)
- 650 Newell-Price, P., Chambers, B., Whittingham, M., 2011. The alleviation of grassland  
651 compaction by mechanical soil loosening. Defra Project BD5001 Final Report.
- 652 Newell Price, B., Chambers, B., Whittingham, M., 2012. Characterisation of Soil Structural  
653 Degradation Under Grassland and Development of Measures to Ameliorate its Impact  
654 on Biodiversity and other Soil Functions. Defra Project BD5001 Final Report.
- 655 Orr, R., Murray, P., Eyles, C., Blackwell, M., Cardenas, L., Collins, A.L., Dungait, J., Goulding,  
656 K., Griffith, B., Gurr, S., Harris, P., Hawkins, J., Misselbrook, T., Rawlings, C.,  
657 Shepherd, A., Sint, H., Takahashi, T., Tozer, K., Whitmore, A.P., Wu, L., Lee, M., 2016.  
658 The North Wyke Farm Platform: effect of temperate grassland farming systems on soil  
659 moisture contents, runoff and associated water quality dynamics. *Eur. J. Soil Sci.*, 67:  
660 374-385. DOI:<https://doi.org/10.1111/ejss.12350>
- 661 Palmer, R.C., Smith, R.P., 2013. Soil structural degradation in SW England and its impact on  
662 surface-water runoff generation. *Soil Use Manag.*, 29: 567-575.  
663 DOI:<https://doi.org/10.1111/sum.12068>
- 664 Pathak, P., Sudi, R., Wani, S.P., Sahrawat, K.L., 2013. Hydrological behavior of Alfisols and  
665 Vertisols in the semi-arid zone: Implications for soil and water management. *Agric.  
666 Water Manag.*, 118: 12-21. DOI:<https://doi.org/10.1016/j.agwat.2012.11.012>
- 667 Perego, A., Wu, L., Gerosa, G., Finco, A., Chiazzese, M., Amaducci, S., 2016. Field evaluation  
668 combined with modelling analysis to study fertilizer and tillage as factors affecting N<sub>2</sub>O  
669 emissions: a case study in Po valley (Northern Italy) *Agric. Ecosyst. Environ.*, 225: 72-  
670 85. DOI:<https://doi.org/10.1016/j.agee.2016.04.003>
- 671 Pulley, S., Collins, A.L., 2019. Field-based determination of controls on runoff and fine  
672 sediment generation from lowland grazing livestock fields. *J. Environ. Manage.*, 249:  
673 109365. DOI:<https://doi.org/10.1016/j.jenvman.2019.109365>
- 674 Rust, W., Corstanje, R., Holman, I.P., Milne, A.E., 2014. Detecting land use and land  
675 management influences on catchment hydrology by modelling and wavelets. *J. Hydrol.*,  
676 517: 378-389. DOI:<https://doi.org/10.1016/j.jhydrol.2014.05.052>
- 677 Schaller, N., Sillmann, J., Müller, M., Haarsma, R., Hazeleger, W., Hegdahl, T.J., Kelder, T.,  
678 van den Oord, G., Weerts, A., Whan, K., 2020. The role of spatial and temporal model  
679 resolution in a flood event storyline approach in western Norway. *Weather and Climate  
680 Extremes*, 29: 100259. DOI:<https://doi.org/10.1016/j.wace.2020.100259>
- 681 Sharma, A., Wasko, C., Lettenmaier, D.P., 2018. If precipitation extremes are increasing, why  
682 aren't floods? *Water Resour. Res.*, 54: 8545-8551.

683 DOI:<https://doi.org/10.1029/2018wr023749>

684 Stevens, A.J., Clarke, D., Nicholls, R.J., 2016. Trends in reported flooding in the UK: 1884–  
685 2013. *Hydrolog. Sci. J.*, 61: 50-63.  
686 DOI:<https://doi.org/10.1080/02626667.2014.950581>

687 Verstraten, L., Wasko, C., Ashford, G., Sharma, A., 2019. Sensitivity of Australian roof  
688 drainage structures to design rainfall variability and climatic change. *Build. Environ.*,  
689 161: 106230. DOI:<https://doi.org/10.1016/j.buildenv.2019.106230>

690 Wasko, C., Sharma, A., Lettenmaier, D.P., 2019. Increases in temperature do not translate to  
691 increased flooding. *Nat. Commun.*, 10: 5676. DOI:<https://doi.org/10.1038/s41467-019-13612-5>  
692

693 Watts, G., Anderson, M., 2016. Water climate change impacts report card 2016.  
694 DOI:<https://nerc.ukri.org/research/partnerships/ride/lwec/report-cards/water/>

695 Wu, L., Bingham, I.J., Baddeley, J.A., Watson, C.A., 2009. Modeling plant nitrogen uptake  
696 using three-dimensional and one-dimensional root architecture. In: Ma, L., Ahuja, L.R.,  
697 Bruulsema, T.W. (Eds.), *Quantifying and understanding plant nitrogen uptake systems*  
698 modeling. CRC Press, Boca Raton, FL, pp. 197-218.

699 Wu, L., Blackwell, M., Dunham, S., Hernández-Allica, J., McGrath, S.P., 2019. Simulation of  
700 phosphorus chemistry, uptake and utilisation by winter wheat. *Plants*, 8: 404.  
701 DOI:<https://doi.org/10.3390/plants8100404>

702 Wu, L., McGechan, M.B., McRoberts, N., Baddeley, J.A., Watson, C.A., 2007. SPACSYS:  
703 integration of a 3D root architecture component to carbon, nitrogen and water cycling  
704 - model description. *Ecol. Model.*, 200: 343-359.  
705 DOI:<https://doi.org/10.1016/j.ecolmodel.2006.08.010>

706 Wu, L., Rees, R.M., Tarsitano, D., Zhang, X., Jones, S.K., Whitmore, A.P., 2015. Simulation  
707 of nitrous oxide emissions at field scale using the SPACSYS model. *Sci. Total Environ.*,  
708 530–531: 76-86. DOI:<http://dx.doi.org/10.1016/j.scitotenv.2015.05.064>

709 Wu, L., Zhang, X., Griffith, B.A., Misselbrook, T., 2016. Sustainable grassland systems: A  
710 modelling perspective based on the North Wyke Farm Platform. *Eur. J. Soil Sci.*, 67:  
711 397-408. DOI:<https://doi.org/10.1111/ejss.12304>

712 Zehe, E., Graeff, T., Morgner, M., Bauer, A., Bronstert, A., 2010. Plot and field scale soil  
713 moisture dynamics and subsurface wetness control on runoff generation in a  
714 headwater in the Ore Mountains. *Hydrol. Earth Syst. Sci.*, 14: 873-889.  
715 DOI:<https://doi.org/10.5194/hess-14-873-2010>

716 Zhang, X., Sun, N., Wu, L., Xu, M., Bingham, I.J., Li, Z., 2016. Effects of enhancing soil organic  
717 carbon sequestration in the topsoil by fertilization on crop productivity and stability:  
718 evidence from long-term experiments with wheat-maize cropping systems in China.  
719 *Sci. Total Environ.*, 562: 247-259. DOI:<https://doi.org/10.1016/j.scitotenv.2016.03.193>  
720

721 **Figure captions**

722 Figure 1. Details of the NWFP catchment selected for this study (catchment number 6 of 15,  
723 consisting of a single field called Golden Rove).

724 Figure 2. Time-series plots for measured and simulated water flux data (not aggregated) for  
725 15-minute, hourly, 6-hourly and daily data (in units of  $\text{mm } 15\text{min}^{-1}$ ,  $\text{mm h}^{-1}$ ,  $\text{mm } 6\text{h}^{-1}$   
726 and  $\text{mm d}^{-1}$ , respectively). All plots are shown with a threshold at the 99th percentile  
727 of measured data (at  $0.138 \text{ mm } 15\text{min}^{-1}$ ,  $0.553 \text{ mm h}^{-1}$ ,  $3.45 \text{ mm } 6\text{h}^{-1}$  and  $14.9 \text{ mm d}^{-1}$ ,  
728 respectively).

729 Figure 3. Scatterplots of the measured and simulated data (not aggregated) for 15-minute,  
730 hourly, 6-hourly and daily data. Scatterplots are shown with the 1:1 line, a linear  
731 regression fit and a loess smoother fit. Units are in  $\text{mm } 15\text{min}^{-1}$ ,  $\text{mm h}^{-1}$ ,  $\text{mm } 6\text{h}^{-1}$  and  
732  $\text{mm d}^{-1}$ , respectively.

733 Figure 4. Time-series plots for daily measured and daily simulated water flux data (with the  
734 first three plots having data aggregated from: 15 minutes to daily; hourly to daily; 6  
735 hourly to daily). All units in  $\text{mm d}^{-1}$ . All plots are shown with a threshold at the 99th  
736 percentile of measured data ( $14.90 \text{ mm d}^{-1}$ ).

737 Figure 5. Scatterplots of the daily measured and daily simulated data (with the first three plots  
738 having data aggregated from: 15 minutes to daily; hourly to daily; 6 hourly to daily).

739 Scatterplots are shown with the ideal 1:1 line, a linear regression fit and a loess  
740 smoother fit. All units in  $\text{mm d}^{-1}$ .

741 Figure 6. Density plots for daily measured and daily simulated data (with the first three plots  
742 having data aggregated from: 15 minutes to daily; hourly to daily; 6 hourly to daily).  
743 All units in  $\text{mm d}^{-1}$ .

744 Figure 7. Error (MAE, NRMSE, PBIAS) indices with respect to daily measured and daily  
745 simulated data (with 15-minute, hourly, 6-hourly data aggregated to daily).

746 Figure 8. Time-series of errors (simulated minus measured data) aggregated to the daily  
747 temporal resolution. All units in  $\text{mm d}^{-1}$ . Positive errors represent over-prediction by  
748 the model.

749 Figure 9. Agreement (NSE,  $d$ , KGE) indices with respect to daily measured and daily  
750 simulated data (with 15-minute, hourly, 6-hourly simulations aggregated to daily).

751